nature physics

SUPPLEMENTARY INFORMATION

DOI: 10.1038/NPHYS3875

Stokes solitons in optical microcavities

Qi-Fan Yang*, Xu Yi*, Ki Youl Yang and Kerry Vahala†

T. J. Watson Laboratory of Applied Physics, California Institute of Technology, Pasadena, California 91125, USA.

*These authors contributed equally to this work.

†Corresponding author: vahala@caltech.edu

DOI: 10.1038/NPHYS3875

I. NUMERICAL SIMULATION

Master equations. The interaction between two solitons via cross phase modulation and the Raman process has been studied in optical fibers using coupled pulse propagation equations[1,2]. This approach is extended to study the Stokes soliton generation process in microresonators. A pair of coupled equations describing the intracavity slowly-varying field amplitudes for the primary and Stokes soliton system can be adapted from the Lugiato-Lefever equation (LL equation)[3–6] augmented by Raman interactions[2], which reads:

$$\begin{aligned}\frac{\partial E_p(\phi)}{\partial t} =& i\frac{D_{2p}}{2}\frac{\partial^2 E_p}{\partial \phi^2} + i(1-f_R)(g_p\left|E_p\right|^2 + 2G_p\left|E_s\right|^2)E_p + i\frac{f_R E_p}{D_{1p}}\int h_R(\frac{\phi-\phi'}{D_{1p}})(g_p\left|E_p(\phi')\right|^2 + G_p\left|E_s(\phi')\right|^2)d\phi' \\ &+ i\frac{f_R E_s}{D_{1p}}\int h_R(\frac{\phi-\phi'}{D_{1p}})G_p E_p(\phi')E_s^*(\phi')\exp(i\Omega\frac{\phi-\phi'}{D_{1p}})d\phi' - (\frac{\kappa_p}{2}+i\Delta\omega_p)E_p + \sqrt{\kappa_p^{ext}P_{in}},\end{aligned} \tag{S1}$$

$$\begin{aligned}\frac{\partial E_s(\phi)}{\partial t} =& -\delta\frac{\partial E_s}{\partial \phi} + i\frac{D_{2s}}{2}\frac{\partial^2 E_s}{\partial \phi^2} + i(1-f_R)(g_s\left|E_s\right|^2 + 2G_s\left|E_p\right|^2)E_s + i\frac{f_R E_s}{D_{1p}}\int h_R(\frac{\phi-\phi'}{D_{1p}})(g_s\left|E_s(\phi')\right|^2 + G_s\left|E_p(\phi')\right|^2)d\phi' \\ &+ i\frac{f_R E_p}{D_{1p}}\int h_R(\frac{\phi-\phi'}{D_{1p}})G_s E_s(\phi')E_p^*(\phi')\exp(-i\Omega\frac{\phi-\phi'}{D_{1p}})d\phi' - (\frac{\kappa_s}{2}+i\Delta\omega_s)E_s.\end{aligned} \tag{S2}$$

The slowly varying fields E_j (subscript $j=(p,s)$ for primary or Stokes soliton) are normalized to optical energy. To second order, the frequency of mode number μ in mode family $j=(p,s)$ is given by the Taylor expansion $\omega_{\mu j}=\omega_{0j}+D_{1j}\mu+\frac{1}{2}D_{2j}\mu^2$ where ω_{0j} is the frequency of mode $\mu=0$, while D_{1j} and D_{2j} are the FSR and the second-order dispersion at $\mu=0$. Ω is the carrier frequency difference $\omega_{0p}-\omega_{0s}$. Also, $\delta=D_{1s}-D_{1p}$ is the FSR difference between primary and Stokes solitons at mode $\mu=0$. κ_j is the cavity loss rate and $\Delta\omega_j$ is the detuning of mode zero of the soliton spectrum relative to the cold cavity resonance. $h_R(t)$ is the Raman response function[2]. For the primary soliton, which is a dissipative Kerr soliton (DKS), the pump field is locked to one of the soliton spectral lines and this "pump" line is taken as mode $\mu=0$. κ_p^{ext} is the external coupling coefficient and P_{in} is the pump power. g_j and G_j are self and cross phase modulation coefficients, defined as,

$$g_j=\frac{n_2\omega_j D_{1j}}{2n\pi A_{jj}},\quad G_j=\frac{n_2\omega_j D_{1j}}{2n\pi A_{ps}}. \tag{S3}$$

where the nonlinear mode area A_{jk} is defined as[2]

$$A_{jk}=\frac{\iint_{-\infty}^{\infty}\left|u_j(x,y)\right|^2dxdy\iint_{-\infty}^{\infty}\left|u_k(x,y)\right|^2dxdy}{\iint_{-\infty}^{\infty}\left|u_j(x,y)\right|^2\left|u_k(x,y)\right|^2dxdy}, \tag{S4}$$

where u_j is the transverse distribution of the mode. $f_R=0.18$ is the Raman contribution parameter in silica.

Adiabatic approximation. As the pulse width of the solitons in our system is several hundred femtosecond, which is much longer than the Raman response time ($\sim$ 10 fs), the pulse fields E_p and E_s can be considered slowly varying variables when compared with $h_R(t)$. Therefore, the integrals of E_p and E_s in eqns. (S1) and (S2) associated with Raman response function can be expanded into a Taylor series by writing $\phi'=\phi-(\phi-\phi')$:

$$\int h_R(\frac{\phi-\phi'}{D_{1p}})\left|E_j(\phi-(\phi-\phi'))\right|^2d\phi' \approx \left|E_j(\phi)\right|^2 - D_{1p}\frac{\partial\left|E_j(\phi)\right|^2}{\partial\phi}\int\tau h_R(\tau)d\tau \tag{S5}$$

$$\int h_R(\frac{\phi-\phi'}{D_{1p}})E_j(\phi-(\phi-\phi'))E_k^*(\phi-(\phi-\phi'))e^{-i\Omega\frac{\phi-\phi'}{D_{1p}}}d\phi' \approx E_j(\phi)E_k^*(\phi)\int h_R(\tau)e^{-i\Omega\tau}d\tau \tag{S6}$$

where $\tau=(\phi-\phi')/D_{1p}$. The next highest order term in eqn. (S6) is found to have a negliible effect on simulation and is neglected here. Using these approximate forms, the coupled equations simplify as follows:

$$\frac{\partial E_p}{\partial t} = i\frac{D_{2p}}{2}\frac{\partial^2 E_p}{\partial \phi^2} + i[g_p|E_p|^2 + (2-f_R)G_p|E_s|^2]E_p - iD_{1p}\tau_R E_p\frac{\partial(g_p|E_p|^2 + G_p|E_s|^2)}{\partial\phi} - (\frac{\kappa_p}{2} + i\Delta\omega_p)E_p - \frac{\omega_p}{\omega_s}R|E_s|^2E_p + \sqrt{\kappa_p^{ext}P_{in}}, \quad \text{(S7)}$$

$$\frac{\partial E_s}{\partial t} = -\delta\frac{\partial E_s}{\partial\phi} + i\frac{D_{2s}}{2}\frac{\partial^2 E_s}{\partial\phi^2} + i[g_s|E_s|^2 + (2-f_R)G_s|E_p|^2]E_s - iD_{1p}\tau_R E_s\frac{\partial(g_s|E_s|^2 + G_s|E_p|^2)}{\partial\phi} - (\frac{\kappa_s}{2} + i\Delta\omega_s)E_s + R|E_p|^2E_s. \quad \text{(S8)}$$

where $R = f_R G_s \mathrm{Im}[\int h_R(\tau)\exp(i\Omega\tau)d\tau] = cD_{1p}g_R(\omega_s,\omega_p)/4n\pi A_{ps}$ and $g_R(\omega_s,\omega_p)$ is the Raman gain in silica. The Raman shock time is defined by $\tau_R = f_R\int \tau h_R(\tau)d\tau$ and is $\sim$ 2-3 fs in silica. For solitons with a few THz bandwidth, other effects are negligible (e.g., higher order dispersion, the self-steepening effect and Raman induced refractive index change[2]). If the soliton pulse width is well below 100 fs, i.e., it has a broadband spectrum, then the coupled equations with higher-order Raman correction might be required.

Phase locking terms. Phase-sensitive, four-wave-mixing terms have also been omitted in Eqn. (S7) and (S8). In principle, these terms could introduce locking of the Stokes and primary soliton fields (in addition to their repetition rates). However, for this to occur the underlying spatial mode families would need to feature mode frequencies that align reasonably well (both in FSR and offset frequency) within the same band. In this work, the mode frequences were observed to not overlap using devices that featured spectrally overlapping solitons.

II. THEORETICAL ANALYSIS (WEAK STOKES LIMIT)

Although an exact solution of the coupled solitons cannot be obtained, the near threshold behavior of the Stokes soliton can still be studied analytically. In this limit, the primary soliton is unperturbated by the Stokes soliton since the Stokes soliton is weak (i.e., near threshold). Its solution is therefore given by the Sech^2 DKS solution[6]. The Stokes soliton equation then uses this solution for the primary soliton. By selecting the carrier frequency of the Stokes soliton such that $\delta = 0$, the equation for the Stokes soliton can be simplified to the following,

$$\frac{\partial E_s}{\partial t} = i\frac{D_{2s}}{2}\frac{\partial^2 E_s}{\partial\phi^2} + i(2-f_R)G_s|E_s|^2E_s - (\frac{\kappa_s}{2} + i\Delta\omega_s)E_s + R|E_p|^2E_s, \quad \text{(S9)}$$

where $E_p = A\mathrm{sech}B\phi$ is the uncoupled primary soliton solution[6] with $|A|^2 = 2\Delta\omega_p/g_p$ and $B = \sqrt{2\Delta\omega_p/D_{2p}}$. The Raman terms containing derivatives cause soliton self frequency shift and subsequently a phase change[7]. However, they minimally affect pulse width and peak power[8,9]. As the primary soliton and Stokes soliton have no abolute phase coherence, these terms have been omitted. Accordingly, the Stokes soliton is treated as a wave trapped in a sech^2-shape potential well created by the primary soliton, and also deriving optical gain from the primary soliton. The bounded solution of the wave function in such a potential has the following form,

$$E_s = V\mathrm{sech}^\gamma B\phi, \quad \text{(S10)}$$

where, consistent with the near threshold assumption, V is a small amplitude satisfying $|V|^2 \ll |A|^2$. Under these assumptions, the exponent γ is a root of the following equation,

$$\gamma(\gamma+1) = 2(2-f_R)G_sD_{2p}/g_pD_{2s}. \quad \text{(S11)}$$

As a physical check of this equation, we note that under circumstances of $G_s = g_p/2$ the potential well created by the primary soliton for the Stokes soliton is identical to the primary soliton potential well (note: the factor of 1/2 comes about from cross phase modulation). In this case, assuming identical second-order dispersion ($D_{2s} = D_{2p}$) and also $f_R = 0$, the solution to eqn. (S11) is $\gamma = 1$ which shows that the Stokes soliton aquires the same envelope as the primary soliton.

Threshold calculation. Once the peak power of the primary soliton reaches a point that provides sufficient Raman gain to overcome Stokes soliton roundtrip loss, the Stokes soliton will begin to oscillate. The threshold condition emerges as the condition for steady-state Stokes soliton power balance. This is readily derived from the Stokes soliton

DOI: 10.1038/NPHYS3875

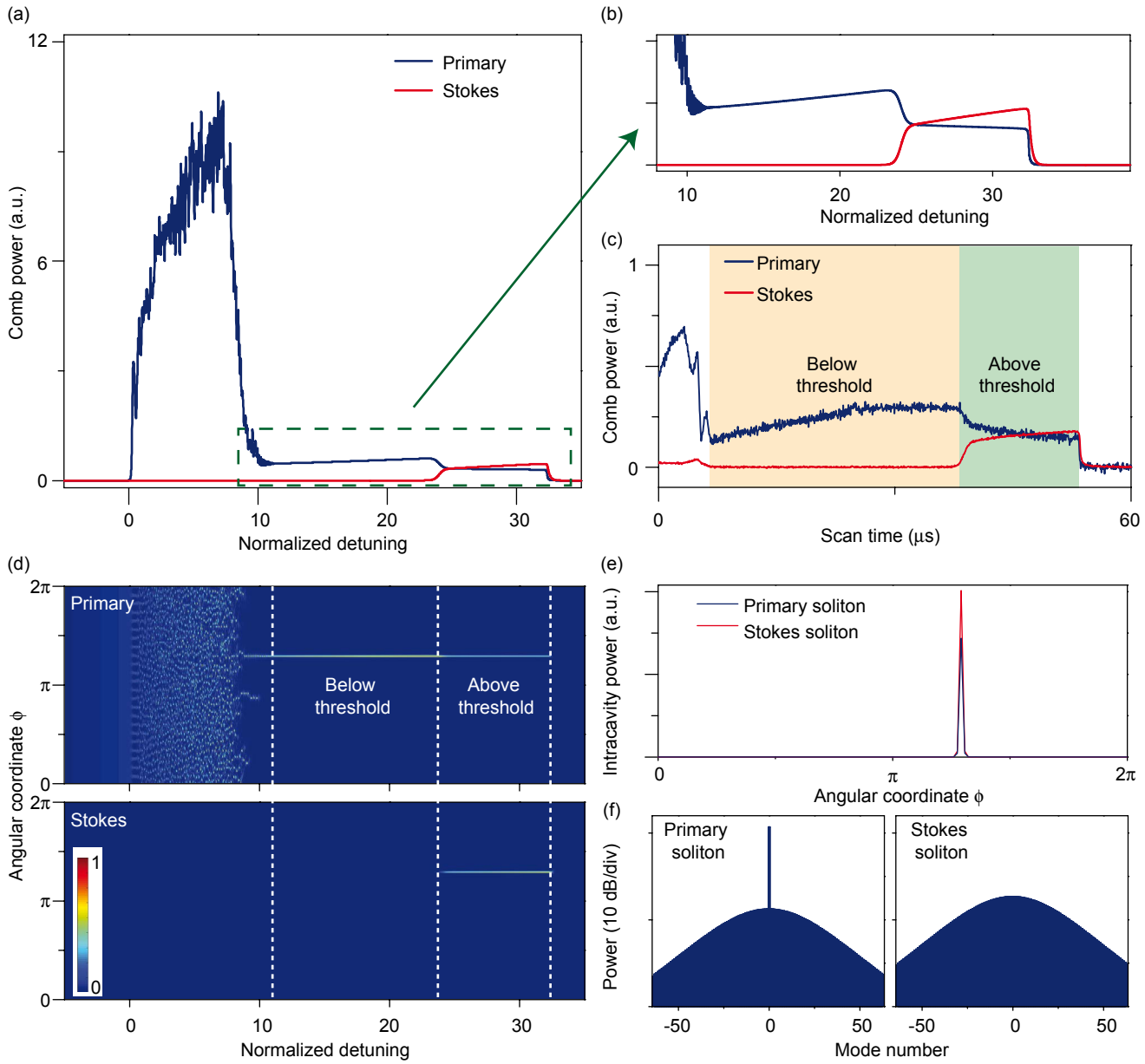

FIG. S1: **Stokes soliton formation in a microresonator. a)** Simulated intracavity comb power during a laser scan over the primary soliton pumping resonance from the blue (left) to the red (right) of the resonance. The detuning is normalized to the resonance linewidth. The initial step corresponds to the primary soliton formation, and the subsequent decrease in power corresponds to the onset of the Stokes soliton. The Stokes soliton power is shown in red. **b)** Zoomed-in view of the indicated region from figure S1(a). **c)** Experimentally measured primary and Stokes soliton power during a laser scan showing the features simulated in S1(a) and S1(b). **d)** Simulation of the intracavity field in the moving frame of the solitons plotted versus the pump laser detuning. The detuning axis is scaled identically to figure S1(a). The figure shows the primary soliton step region (below threshold) as well as the onset of the Stokes soliton (above threshold). **e)** Temporal overlap of the primary and Stokes solitons is numerically confirmed in the plot of normalized power versus location angle within the resonator. The overlap confirms trapping and co-propagation. **f)** Intracavity optical spectra of the primary and Stokes solitons.

equation and takes the form,

$$\int_0^{2\pi} \partial_t |E_s|^2 d\phi = \int_0^{2\pi} d\phi(\kappa_s - 2R|E_p|^2)|E_s|^2 = 0 \tag{S12}$$

By substituting the solutions for the primary and Stokes solitons into eqn. (S12), the resulting threshold in primary soliton peak output power is found to be given by eqn. (1) in the main text.

Background field. A continuous background field exists as part of the primary soliton (DKS) solution. In principle, this constant backgound could induce laser oscillation through the Raman process. However, the threshold power for this to occur can be shown to be close to the peak power required for Stokes soliton oscillation. Moreover, the background field has a power level that is many orders weaker than the peak power of the primary soliton[6]. This results because the pump laser is far red detuned from the microcavity resonance. As a result of these considerations, the observed Stokes oscillation results from pumping by the primary soliton and, specifically, spatio-temporal overlap of the Stokes soliton with the primary (pump) soliton. The good agreement between measurement with the theoretical threshold (eqn. (1) in the main text) provides additional confirmation.

III. FORMATION OF STOKES SOLITON

To reveal further details on the Stokes soliton formation, a pumping laser scan is performed numerically as shown in Fig. S1(a) (and zoom-in of scan in Fig. S1(b)). 128 modes are employed in the simulation. The formation of a step in the primary comb power (blue) indicates primary soliton formation[6,8]. However, a decrease in power of the primary soliton is next observed that occurs with an increase in power of the Stokes soliton (red). The same features are also observed experimentally (see Fig. S1(c)). By studying the intracavity field evolution, the simulation shows the correspondence between these features and the soliton formation (see Fig. S1(d)). Also, the simulation shows that the primary and Stokes pulses overlap in space and time, i.e., confirmation of optical trapping (see figure S1(e)). The calculated spectra for the primary and Stokes solitons are provided in figure S1(f).

There is also a supplementary movie of these results.

[1] Headley, C. & Agrawal, G. P. Unified description of ultrafast stimulated raman scattering in optical fibers. *JOSA B* **13**, 2170–2177 (1996).

[2] Agrawal, G. P. *Nonlinear fiber optics* (Academic press, 2007).

[3] Lugiato, L. A. & Lefever, R. Spatial dissipative structures in passive optical systems. *Phys. Rev. Lett.* **58**, 2209 (1987).

[4] Matsko, A. *et al.* Mode-locked kerr frequency combs. *Opt. Lett.* **36**, 2845–2847 (2011).

[5] Chembo, Y. K. & Menyuk, C. R. Spatiotemporal lugiato-lefever formalism for kerr-comb generation in whispering-gallery-mode resonators. *Phys. Rev. A* **87**, 053852 (2013).

[6] Herr, T. *et al.* Temporal solitons in optical microresonators. *Nature Photon.* **8**, 145–152 (2014).

[7] Karpov, M. *et al.* Raman self-frequency shift of dissipative kerr solitons in an optical microresonator. *Physical review letters* **116**, 103902 (2016).

[8] Yi, X., Yang, Q.-F., Yang, K. Y., Suh, M.-G. & Vahala, K. Soliton frequency comb at microwave rates in a high-q silica microresonator. *Optica* **2**, 1078–1085 (2015).

[9] Yi, X., Yang, Q.-F., Yang, K. Y. & Vahala, K. Theory and measurement of the soliton self-frequency shift and efficiency in optical microcavities. *Optics Letters* **41**, 3419–3422 (2016).